Calculations of a high-gain recombination x-ray laser at 4.55 nm

J. Zhang,[1] M. H. Key,[1,2] S. J. Rose,[2,3] and G. J. Tallents[4]
[1]*Department of Atomic and Laser Physics, University of Oxford, Oxford OX1 3PU, United Kingdom*
[2]*Science and Engineering Research Council, Rutherford Appleton Laboratory, Chilton Didcot Oxon, OX11 0QX, United Kingdom*
[3]*Department of Physics and Space Science, University of Birmingham, Birmingham B15 2TT, United Kingdom*
[4]*Department of Physics, University of Essex, Colchester CO4 3SQ, United Kingdom*
(Received 23 April 1993; revised manuscript received 29 November 1993)

Detailed theoretical investigations of a hydrogenlike magnesium recombination laser at 4.55 nm (the $n=3\rightarrow 2$ Balmer α transition) produced by psec and sub-psec laser pulses irradiating fiber targets are presented. Shorter pulses are shown to produce larger x-ray laser gain with less pumping laser energy.

PACS number(s): 42.60.By, 32.30.Rj, 32.70.−n, 52.50.Jm

I. INTRODUCTION

X-ray laser research has made rapid progress in decreasing the wavelength and increasing the energy output of lasing transitions since the first demonstration of a high-gain amplifier in the soft-x-ray spectral region [1,2]. Collisional excitation in neonlike or nickellike ions and recombination into hydrogenlike or lithiumlike ions are the most successful schemes in the development of x-ray lasers. By using the collisional excitation scheme, amplification has been observed at wavelengths as short as 3.56 nm in nickellike gold ions [3]. Gain saturation has been reached at wavelengths around 20 nm in neonlike germanium and selenium ions [4,5]. Experiments that use the x-ray laser in the area of holography and microscopy have started [6,7]. However, the current collisional excitation scheme would require about a 10-kJ driver energy for saturated and diffraction limited x-ray laser operation in the water window. It is clear that reducing the size and cost of x-ray lasers will be an important step towards increasing their potential applications.

Recombination x-ray lasers operating with adiabatic cooling are of continuing interest because they require a much lower driver energy than collisionally pumped lasers [8–14]. The driver energy requirement of recombination lasers reduces when shorter laser pulses and narrower fiber targets are used.

X-ray lasers with wavelengths near 4.5 nm are optimum for making x-ray holograms of biological structures in living cells as the absorption contrast between carbon (protein) and oxygen (water) is greatest here [6]. The $n=3\rightarrow 2$ (Balmer α) transition in the hydrogenlike magnesium ion is at 4.55 nm and much effort has been dedicated to investigating the hydrogenlike magnesium recombination x-ray laser. However, significant amplification on the Balmer α transition in hydrogenlike magnesium is still unproved [14–17]. Theoretical and experimental studies have indicated that high-gain operation could be possible when shorter driving laser pulses and narrower targets are used [15,18–21]. The availability of psec and sub-psec pulse chirped pulse amplification (CPA) beam on several high-energy Nd glass laser facilities now offers the possibility of further investigation of this lasing process [22,23].

In this paper we present a systematic theoretical study of the recombination x-ray laser operating on the Balmer α transition of hydrogenlike magnesium and show the potential advantages for the recombination x-ray laser driven by psec and sub-psec laser pulses. In particular, our theoretical investigations suggest significant improvement in gain performance of the recombination x-ray laser.

II. BACKGROUND AND COMPUTER CODES

In the hydrogenlike recombination x-ray laser scheme, a fully stripped plasma generated by short-laser-pulse irradiation is rapidly cooled by adiabatic expansion. Electrons preferentially recombine via three-body collisions into the upper levels of hydrogenlike ions. If the expansion is sufficiently rapid, the adiabatic cooling of the plasma may induce population inversion between the $n=3$ and 2 levels of the H-like ions during the recombination cascade by the rapid radiative depletion of the $n=2$ level (the Lyman α resonance transition).

The optimum recombination laser operation relies on production of maximum inversion density when local thermodynamic equilibrium (LTE) conditions prevail for levels above $n=3$, and the $n=2$ level is depopulated mainly by radiative decay. This condition is reached at a density scaling as Z^7 at a later time when lasing gain appears (laser time). This can be understood by considering the ratio of radiative decay of the upper lasing level ($n=3$), which is proportional to Z^4, to the collisional mixing rate, which is proportional to $N_e Z^{-3}$. This ratio scales as $Z^7 N_e$. As Z increases, N_e should increase as Z^7 in order to maintain the same relationship between radiative and collisional processes. The actual electron density initially formed in steady-state laser-driven ablation scales only as Z, therefore the initial density needs to be greatly increased to achieve the optimum operation mode of hydrogenlike magnesium recombination lasers.

The initial density of the plasma can be enhanced by irradiating targets with shorter pulses [14,15,18–20]. When the laser pulse duration is less than the hydrodynamic response time, hydrodynamic motion of the

plasma is insignificant during the pulse, and electron thermal conduction heats the target at close to solid density. This is in contrast to steady-state ablation with long-pulse (nsec) lasers where the main heating occurs close to the critical density, which depends on the laser wavelength at λ^{-2} and is typically two to three orders of magnitude lower than solid density.

Thin fiber targets irradiated in line focus geometry have the additional benefits of two-dimensional rapid cooling as well as a reduction in trapping of Lyman α resonance radiation because of the cylindrical expansion [24]. The end result is that lower temperature can be employed giving a higher population in the $n=3$ upper state of the laser transition [23,25,26].

A one-dimensional Lagrangian hydrodynamic code, MEDUSA, coupled to an atomic physics code, NIMP, are used [27,28] to simulate the behavior of the targets under irradiation. In the simulation, the laser energy is absorbed via inverse bremsstrahlung and resonance absorption. The resonance absorption fraction is set at each time step by calculating the scale length [27] at critical density. Twenty percent of the resonantly absorbed energy is assumed to be dumped at critical density. The rest is put into hot electrons which are transported in ten energy groups with an initial temperature at critical density. Energy transport by thermal electrons (including a 0.1 flux limiter taken from Ref. [29] to represent heat transport in regions of high-temperature gradient), radiation cooling and recombination heating are treated.

The time-dependent atomic physics of all ion stages are modeled in a non-LTE average-atom description. Resonance linewidths are Doppler except for H-like C where Stark broadening of the Balmer α line is calculated. Radiation transfer in the resonance lines is treated by using an escape factor, which accounts for Doppler decoupling [28]. The escape factor is applied separately to each Lagrangian cell with the average velocity gradient taken from the hydrodynamic simulation [28]. As before [30], a maximum multiplier [28] of the optical depth in the escape factor is used in all these simulations to give a lower limit of results. Excited states of hydrogenic ions are treated by rate equations for levels up to $n=10$ with higher levels in LTE with the continuum. Laser gain is evaluated for the Balmer α line with consideration of its fine structure [28].

For ultrashort pulse irradiation collisional absorption is weak due to the small depth of plasma at the critical density. Resonance absorption at the critical density is then the major absorption mechanism [18,31].

The code (or earlier versions of it) has been used extensively in cylindrical geometry to describe the recombination laser gain for fiber targets and it has also been tested in predicting the performance of experimental targets in several previous experiments [10,13,32,33], which used pulse lengths of 10 psec or greater. It has not been tested in the parameter space discussed in this article. However, our present research mainly concentrates on the case of psec laser pulses, which is close to the tested regime. The discussion of the sub-psec pulses poses an exciting challenge to the models in the code, and thus the results predicted for this regime should be taken with an appropriate amount of caution.

III. OPTIMIZATION OF LASING GAIN FOR ULTRASHORT PULSE DRIVERS

Optimized conditions are calculated for 7-μm-diam fibers irradiated by short pulse drivers with various pulse lengths. It has been found experimentally that 7-μm-diam fibers are the thinnest that can be self-supporting and remain straight for lengths up to 1 cm [10,32]. Consequently such targets have the optimum practical diameter for x-ray laser action. Figures 1 and 2 illustrate the computed peak gain coefficient (time resolved and space resolved) as functions of absorbed energy at the 7-μm-diam fiber surface for short-pulse drivers with wavelengths of 1.053 μm and 0.268 μm, respectively. The calculation is one-dimensional and the energy incident at the target surface is varied to find optimum conditions giving the maximum gain. For each combination of the driving pulse length and wavelength, there is a corresponding optimum absorbed energy. For too small an absorbed energy, the plasma temperature is not sufficient to give the early predominant population of bare nuclei that is the necessary starting point of the recombination laser process. If the energy is too large, the LTE populations of the higher excited states are reduced by the increased temperature, which results in reduced population of the upper level and leads to a smaller gain.

The optimum absorbed energy increases with pulse length for both wavelengths. The optimum operation of the recombination lasers driven by the longer wavelength needs higher absorbed energy than that driven by a shorter wavelength with the same pulse duration. The value of the maximum peak gain increases as the pulse length is reduced. The relevant optimized conditions for the recombination lasers at the later expansion time when maximum laser gain occurs (x-ray laser time) are summarized in Tables I and II. In the tables, τ is the driving

TABLE I. Optimized plasma parameters at x-ray laser time for 1.053-μm driver.

τ (psec)	G_{peak} (cm^{-1})	E_{abs} (J/cm)	N_e (cm^{-3})	T_e (eV)	Fraction of bare nuclei (%)
0.2	57	24.1	1.9×10^{21}	154	50.3
0.5	47	25.4	2.0×10^{21}	162	48.7
1	43	27.7	1.6×10^{21}	149	45.9
2	35	29.9	1.5×10^{21}	151	44.1
5	21	35.8	1.3×10^{21}	184	58.7
10	10	37.3	1.0×10^{20}	171	50.8

TABLE II. Optimized plasma parameters at x-ray laser time for 0.268-μm driver.

τ (psec)	G_{peak} (cm^{-1})	E_{abs} (J/cm)	N_e (cm^{-3})	T_e (eV)	Fraction of bare nuclei (5)
0.2	59	17.5	2.0×10^{21}	160	51.1
0.5	57	18.0	2.0×10^{21}	164	49.4
1	55	21.9	1.7×10^{21}	158	53.4
2	48	30.6	1.6×10^{21}	174	60.1
5	24	34.4	1.5×10^{21}	184	59.4
10	11	35.0	1.2×10^{21}	183	56.2

pulse length and G_{peak} the computed peak gain coefficient for time-resolved and space-resolved measurements. E_{abs} is the absorbed energy at the fiber surface assuming a cylindrically symmetric irradiation. N_e and T_e represent the electron density and temperature at peak gain, respectively. The fraction of bare nuclei means the fraction of fully stripped nuclei in the plasma, under the plasma conditions of peak gain.

In Fig. 3 we consider the case of a 7-μm-diam fiber target irradiated by a 1-psec 0.268-μm CPA beam with an optimized absorbed energy of 21.9 J/cm in the plasma. Figure 3 shows a typical example for an optimized simulation of the time evolution of electron temperature (T_e), electron density (N_e), the fraction of fully stripped nuclei, and peak gain for the hydrogenlike magnesium recombination laser at 4.55 nm in the Lagrangian cell, which gives maximum gain (both in time and space resolved). During the 1-psec interaction, there is a very rapid rise in temperature and very steep electron density gradients are produced. The electron temperature increases abruptly to a peak of 1.6 keV during the interaction and after the interaction the plasma expands quickly and the temperature drops rapidly to a plateau in a time less than 10 psec. The gain reaches the maximum when $N_e=1.7\times10^{21}$ cm^{-3} and $T_e=158$ eV. The FWHM (full width at half maximum) time duration of the gain region is about 21 psec with a maximum value occurring at 12.5 psec. Similar results are found for the corresponding calculations for a 1-psec 1.053-μm laser pulse.

The spatial gain profiles are shown in Fig. 4 at 7.0, 12.5, 20.0, and 32.0 psec after the start of the laser pulse under the same conditions as in Fig. 3. Gain onset occurs at $T_e=420$ eV after approximately 5.0 psec with very narrow spatial FWHM, whereas the spatial FWHM at the time at the peak gain is 2.5 μm at 12.5 psec. As the plasma expands further, the peak gain coefficient decreases with increasing spatial FWHM. After 32 psec from the start of the laser, the gain coefficient is reduced to 20 cm^{-1} for $N_e\sim2.7\times10^{20}$ cm^{-3} at a temperature of 51 eV. The spatial FWHM at this time is 7 μm. As the absorbed energy in the plasma increases past the optimal value, the peak gain decreases (Fig. 3) with increasing electron temperature and spatial FWHM of the peak gain.

The simulations show that longer driving pulses produce smaller peak gain with larger spatial FWHM. The spatial FWHM corresponding to the maximum peak gain (~10 cm^{-1}) produced by a 10-psec pulse with an optimized absorbed energy is about 60 μm.

Observations on recombination x-ray lasers are intrinsically more difficult to interpret than those based on collisional excitation. The complicating factor is the mask-

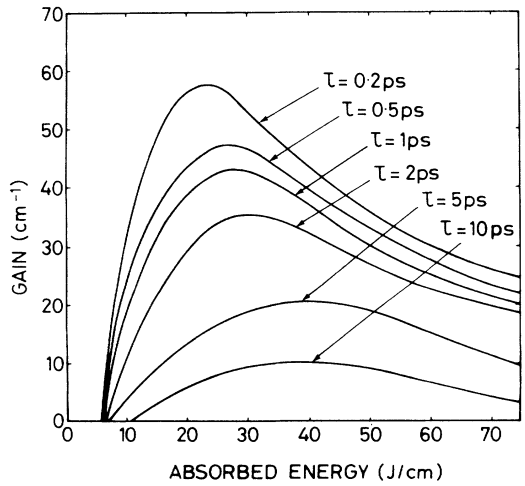

FIG. 1. Peak gain coefficient for time-resolved and space-resolved measurements as functions of absorbed energy for 7-μm-diam magnesium fiber target cylindrically irradiated by 1.053-μm laser pulses.

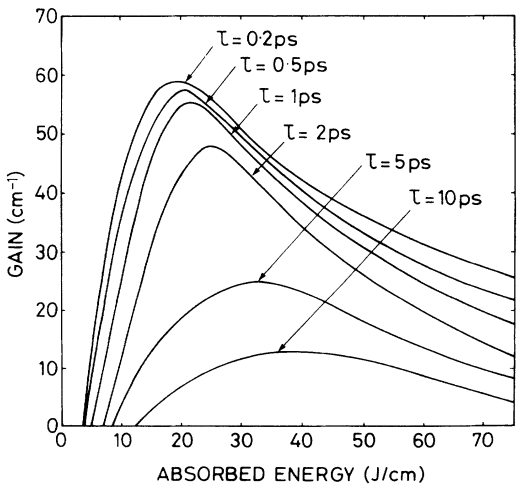

FIG. 2. Peak gain coefficient for time-resolved and space-resolved measurements as functions of absorbed energy for 7-μm-diam magnesium fiber target cylindrically irradiated by 0.268-μm laser pulses.

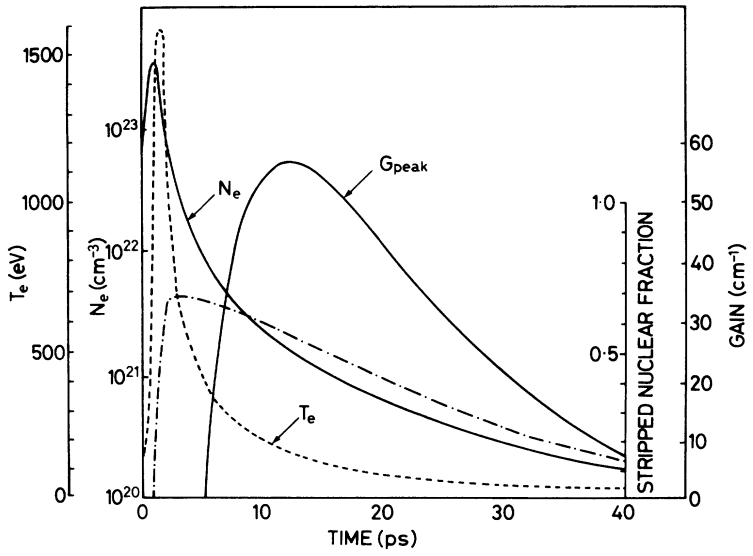

FIG. 3. Time evolution of the electron temperature, the electron density, the fraction of the fully stripped nuclei, and the hydrogenlike magnesium Balmer α (4.55 nm) gain coefficient in the Lagrangian cell which gives maximum peak gain for a 7-μm-diam fiber target cylindrically irradiated by 1-psec 0.268-μm pulse driver with an absorbed energy of 21.9 J/cm.

ing of any gain by nonlasing emission on the laser transition from other space and time regions particularly at higher density and pressure in which amplification does not occur. As a result, the effective gain deduced using the Linford formula from space and (or) time integrated axial to transverse intensity ratios, or from variation of intensity with plasma length, can be substantially different from the peak gain in the case of low-gain-length product. Isolating the gain zone emission from the bulk plasma emission in space and time (to prevent the amplified spontaneous emission being swamped by the bulk spontaneous emission) greatly reduces the difference between the effective and peak gains [15]. For emission from high-gain-length-product plasma, the relative difference becomes less important. The temporal distribution of the effective gain (spatially integrated and time resolved) with the optimized absorbed energy for the magnesium fiber target irradiated cylindrically by the 1-psec pulse driver is illustrated in Fig. 5. The effective gain is calculated from the nonlinear increase from the 2.5-mm length of the spatially integrated axial intensity using the Linford formula [34]. This effective gain is what is measured experimentally by spatially integrated and time-resolved spectroscopy along the axis of the target [32].

IV. COOLING CHARACTERISTICS OF RECOMBINING PLASMAS

In the recombination laser scheme presented here, short CPA pulses heat the fiber surface and ionize the atoms in the surface layer of fibers to bare nuclei. In the heating phase plasma is formed from the surface of the fiber [23,25]. During the subsequent adiabatic expansion, recombination into H-like ions leads to population inversion and gain.

The initial plasma conditions and the cooling characteristics are important features in the recombining plasma determining the lasing gain. Figures 6 and 7 show the initial plasma conditions and the conditions when x-ray lasing occurs in the optimum Lagrangian cell for different ultrashort pulse drivers with the optimized absorbed en-

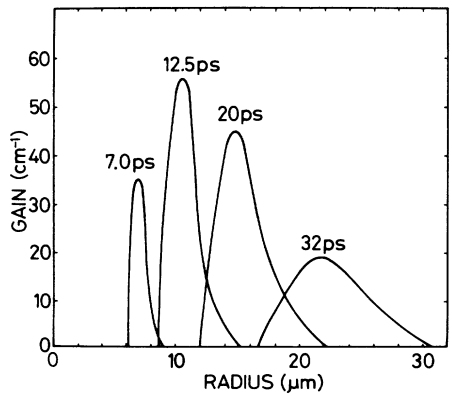

FIG. 4. Spatial gain profile of hydrogenlike magnesium recombination laser calculated at 7.0, 12.5, 20.0, and 32.0 psec after the start of the laser pulse under the same conditions as in Fig. 3.

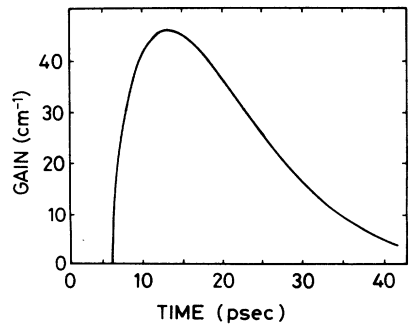

FIG. 5. Time evolution of the spatially integrated gain of the hydrogenlike magnesium recombination laser under the same conditions as in Fig. 3

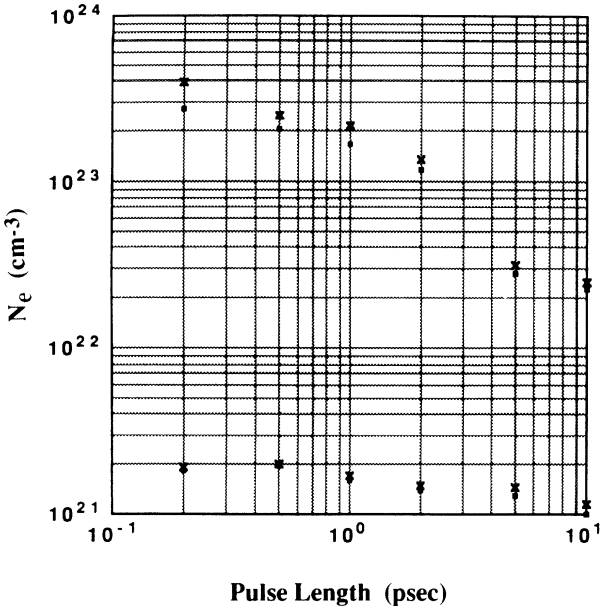

FIG. 6. Variations of the initial electron density and the electron density at x-ray laser time in the optimum Lagrangian cell with the pulse length for 1.053-μm (●) and 0.268-μm (×) wavelengths, respectively (the absorbed energy is optimized separately for each pulse length).

ergy. The simulations show that maximum lasing gain always occurs with approximately the same plasma conditions in the cells exhibiting gain, i.e., $N_e \sim (1.0-2.0)\times 10^{21}$ cm^{-3} and $T_e \sim 155-185$ eV. The initial peak electron density at optimum irradiation intensity decreases almost linearly with pulse length. The initial electron temperature at optimum irradiation intensity (defined as the peak electron temperature at the early heating period) has a weak dependence on the driving pulse length. As the pulse length increases, the optimum initial temperature decreases slightly.

The recombination rate and gain depend strongly on the plasma cooling rate. Increased cooling rate leads to reduced temperature at the optimized electron density and then to induce larger density of inverted population for the Balmer α transition and consequently induce higher lasing gain. In order to illustrate the dependence of the cooling rate on the driving laser pulse length, the cooling time from the initial temperature to the temperature at x-ray laser time is shown against the driving pulse length (Fig. 8). It can be seen in Fig. 8 that the plasmas produced by the 0.268-μm wavelength laser driver cools more rapidly and that the difference between the cooling rates for 1.053-μm and 0.268-μm pulse drivers becomes the largest for the drivers with pulse lengths between 500 fsec and 2 psec. This explains why the lasing gains produced by the 0.268-mm pulse driver are about 20% larger than those produced by the 1.053-μm pulse driver with the pulse length in the range between 500 fsec and 2 psec (see Tables I and II).

The initial depth of the optimum Lagrangian cell from the surface of the fiber target has been computed for different driving pulse lengths. An example of the dependence of the initial depth on the irradiance for 1-psec driving pulses is shown in Fig. 9. The Lagrangian cell, which is initially 30 nm from the target surface, with the optimum conditions of $N_e \sim (1.6-1.7)\times 10^{21}$ cm^{-3} and $T_e \sim 150-158$ eV at the x-ray laser time, mainly contributes to the amplification. The plasma, which comes from initial depths closer to the surface, expands too fast for attaining optimum density and temperature. Initial depths less than 10 nm do not contribute to the amplification. In contrast, the plasma initially too far from the surface cannot reach a temperature high enough to achieve sufficient ionization. the optimum initial depth against the driving pulse length is plotted in Fig. 10. For shorter driving pulse, the initial depth is smaller.

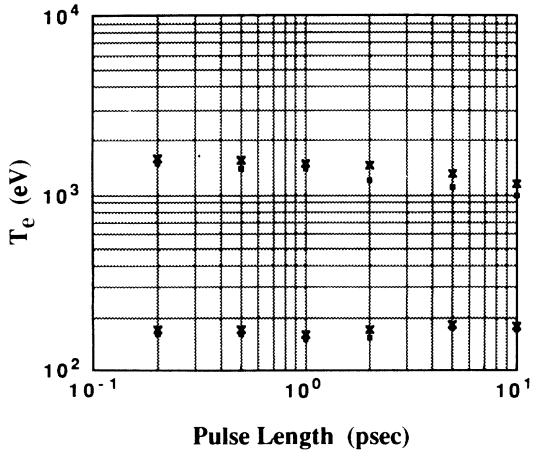

FIG. 7. Variations of the initial electron temperature and the electron temperature at x-ray laser time in the optimum Lagrangian with the driving pulse length for 1.053-μm and (●) 0.268-μm (×) wavelengths, respectively (absorbed energy is optimized separately for each pulse length).

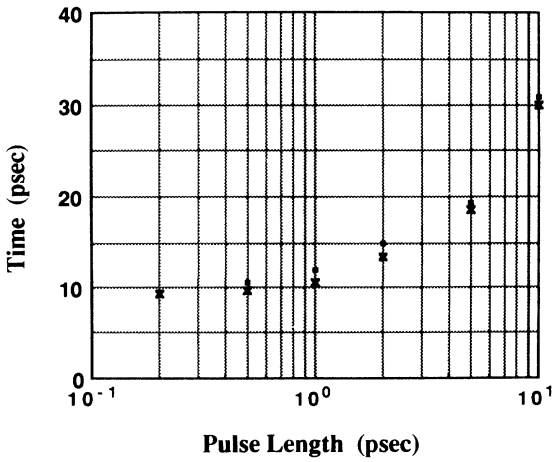

FIG. 8. Variations of the cooling time taken the initial electron temperature to the required temperature for optimum lasing operation with the driving pulse length for 1.053-μm (●) and 0.268-μm (×) wavelengths, respectively.

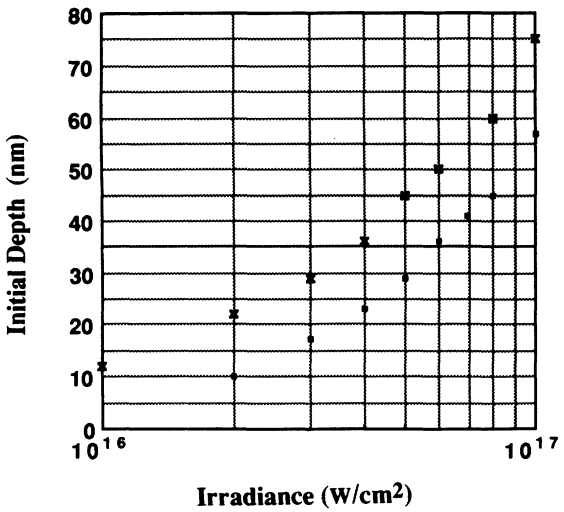

FIG. 9. Initial depth of the optimum Lagrangian cell from the surface of the fiber target against the irradiance on the surface of the target irradiated by 1-psec pulse drivers with 1.053-μm (●) and 0.268-μm (×) wavelengths.

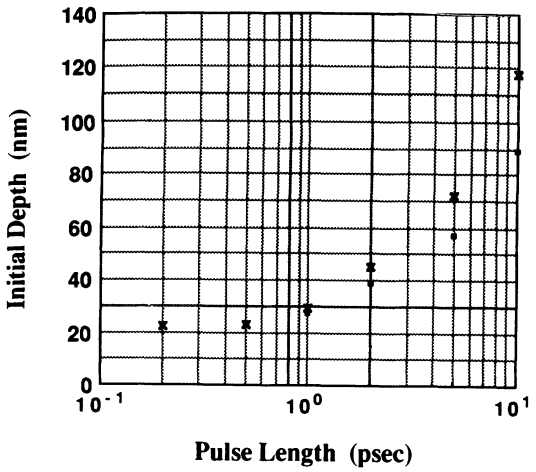

FIG. 10. Initial depth of the optimum Lagrangian cell from the surface of the fiber target against the driving pulse length for 1.053-μm (●) and 0.268-μm (×) wavelengths.

The smallest optimum initial depth is 20 nm for sub-psec pulse drivers. For the longer pulse drivers, the optimum lasing operation requires greater initial depths for the 0.268-μm wavelength drivers than for the 1.053-μm drivers.

There is no significant hydrodynamic motion of the plasma during the psec and sub-psec ultrashort pulses and thermal electron conduction dominates the energy transport process. At the end of the laser irradiation, a body of plasma is formed with large density and temperature gradients. Rapid cooling starts immediately becuase of rapid electron thermal conduction into the bulk of the solid and the rapid adiabatic expansion into the vacuum. If the inner portion of the plasma had larger conductivity than the outer portion, faster cooling could be achieved. It is therefore interesting to study the effect of increasing the cooling rate by substituting materials under the lasing layer producing plasma of higher conductivity.

It should be noted that the effects of imbedding a plasma filament in a cold background plasma to increase the thermal conduction cooling have been explored theoretically [35]. Thermal conduction has been shown to be very effective in cooling the plasma filament in that case. However, imbedding a plasma filament in another cold background plasma seems hard to be implemented experimentally and the cold background plasma will influence adiabatic expansion of the plasma filament. Cylindrical targets with a higher conductivity layer under the lasing layer is, however, easier to achieve and has the benefits of increasing the thermal conduction into the bulk of solid as well as inhibiting adiabatic cooling.

At the early time of heating, the plasma experiences very rapid heating. After the termination of the laser irradiation, rapid cooling can be divided into two stages dominated by thermal conduction and expansion cooling, respectively. At the first stage of the cooling, thermal conduction predominates over expansion cooling becuase the sufficiently high initial temperature and small initial size of the plasma [35]. Thermal conductivity in the initial plasma can be orders of magnitude greater than that of a room-temperature solid [36].

V. CONCLUSIONS

In summary, we have presented a detailed investigation of the hydrogenlike magnesium recombination laser driven by psec and sub-psec ultrashort pulses. Significant improvement of gain performance of the recombination lasers at 4.55 nm has been shown using the ultrashort pulse drivers. The optimized initial depth, which corresponds to the plasma cell where maximum gain occurs at a later expansion period, from the surface of the fiber is found to be small (several tens of nm) for the ultrashort-pulse-laser drivers. Cooling characteristics of the recombining plasmas are studied. Thermal electron conduction predominates over expansion cooling at early stages. Saturated gain operation requires a high-gain-length product. The calculations presented here, however, do not include the effects caused by nonuniform irradiation along the plasma length. However, our recent research shows that increasing the irradiation intensity can avoid the production of absorbing zones along the plasma length and lessen the problem of mismatch of the space-time gain windows of the hydrogenlike magnesium recombination x-ray laser [37]. It would therefore be expected that a significant gain-length product might be achieved using this scheme.

[1] D. L. Matthews, P. L. Hagelstein, M. D. Rosen, M. J. Eckart, N. M. Ceglio, A. U. Hazi, H. Medecki, B. J. MacGowan, J. E. Trebes, B. L. Whitten, E. M. Campbell, C. W. Hatcher, A. M. Hawryluk, R. L. Kauffman, L. D. Pleasance, G. Rambach, J. H. Scofield, G. Stone, and T. A. Weaver, Phys. Rev. Lett. **54**, 110 (1985).

[2] M. D. Rosen, P. L. Hagelstein, D. L. Matthews, E. M. Campbell, A. U. Hazi, B. L. Whitten, B. MacGowan, R. E. Turner, and R. W. Lee, Phys. Rev. Lett. **54**, 106 (1985).

[3] B. J. MacGowan, L. B. Da Silva, D. J. Fields, C. J. Keane, J. A. Koch, R. A. London, D. L. Matthews, S. Maxon, S. Mrowka, A. L. Osterheld, J. H. Scofield, G. Shimkaveg, J. E. Trebes, and R. S. Walling, Phys. Fluids B **4**, 2326 (1992).

[4] A. Carillon, H. Z. Chen, P. Dhez, L. Dwivedi, J. Jacoby, P. Jaegle, G. Jamelot, J. Zhang, M. H. Key, A. Kidd, A. Krisnick, R. Kodama, J. Krishnan, C. L. S. Lewis, D. Neely, P. Norreys, D. O'Neill, G. J. Pert, S. A. Ramsden, J. P. Raucourt, G. J. Tallents, and J. Uhomoibhi, Phys. Rev. Lett. **68**, 2917 (1992).

[5] J. A. Koch, B. J. MacGowan, L. B. Da Silva, D. L. Matthews, J. H. Underwood, P. J. Batson, and S. Mrowka, Phys. Rev. Lett. **68**, 3291 (1992).

[6] L. B. Da Silva, J. E. Trebes, R. Balhorn, S. Mrowka, E. Anderson, D. T. Attwood, T. W. Barbee, Jr., J. Brase, M. Corzett, J. Gray, J. A. Koch, C. Lee, D. Kern, R. A. London, B. J. MacGowan, D. L. Matthews, and G. Stone, Science **258**, 269 (1992).

[7] R. A. London, M. D. Rosen, and J. E. Trebes, Appl. Opt. **28**, 3397 (1989).

[8] S. Suckewer, C. H. Skinner, H. Milchberg, C. Keane, and D. Voorhees, Phys. Rev. Lett. **55**, 1753 (1985). S. Suckewar, C. H. Skinner, D. Kim, E. Valeo, D. Voorhees, and A. Wouters, Phys. Rev. Lett. **57**, 1004 (1986).

[9] G. Jamelot, A. Klisnick, A. Carillon, H. Guennou, A. Sureau, and P. Jaegle, J. Phys. B **18**, 4647 (1985).

[10] C. Chenais-Popovics, R. Corbett, C. J. Hooker, M. H. Key, G. P. Kiehn, C. L. S. Lewis, G. J. Pert, C. Regan, S. J. Rose, S. Sadaat, R. Smith, T. Tomie, and O. Willi, Phys. Rev. Lett. **59**, 2161 (1987).

[11] Y. Kato, H. Azuma, K. Murai, K. Yamakawa, H. Shiraga, G. J. Pert, S. A. Ramsden, and M. H. Key, in *X-Ray Lasers 1990,* edited by G. J. Tallents (IOP, Bristol, 1991), p. 1.

[12] Z. Z. Xu, P. Z. Fan, Z. Q. Zhang, S. S. Chen, L. H. Lin, P. X. Lu, L. Sun, X. F. Wang, J. J. Yu, and A. D. Qian, in *X-Ray Lasers 1990* (Ref. [11]), p. 151.

[13] M. Grande, M. H. Key, G. Kiehn, C. L. S. Lewis, G. J. Pert, S. A. Ramsden, C. Regan, S. J. Rose, R. Smith, T. Tomie, and O. Willi, Opt. Commun. **74**, 309 (1990).

[14] H. Nishimura, H. Shiraga, H. Daido, T. Tachi, P. R. Herman, E. Miura, H. Takabe, M. Yamanaka, Y. Kato, G. J. Tallents, and M. H. Key, *Short Wave Coherent Radiation: Generation and Applications,* Proceedings of OSA Vol. 20 (Optical Society of America, Washington, DC, 1988), p. 137.

[15] M. H. Key, N. Tragin, and S. J. Rose, in *X-Ray Lasers 1990* (Ref. [11]), p. 163.

[16] R. Shepherd, D. Fields, L. B. Da Silva, C. Keane, B. MacGowen, D. Matthews, G. Shimkaveg, G. Stone, D. Eder, A. Osterheld, R. Walling, B. K. F. Young, A. Fry, M. Eckart, W. Goldstein, R. Stewart, G. Charatis, and G. Bush, in *X-Ray Lasers 1990* (Ref. [11]), p. 13.

[17] D. C. Eder, Phys. Fluids B **2**, 3086 (1990).

[18] N. H. Burnett and P. B. Corkum, J. Opt. Soc. Am. B **6**, 1195 (1989).

[19] D. C. Eder, P. Amendt, and S. C. Wilks, Phys. Rev. A **45**, 6741 (1992).

[20] E. J. Valeo and S. C. Cowley, Phys. Rev. E **47**, 1321 (1993).

[21] F. G. Patterson, M. D. Perry, R. Gonzales, and E. M. Campbell, in *Femtosecond to Nanosecond High-Intensity Lasers and Applications,* edited by E. M. Campbell, SPIE Proc. Vol. 1229 (SPIE, Bellingham, WA, 1990), p.2.

[22] C. N. Danson, L. Barzanti, Z. Chang, A. Damerell, M. D. Dooley, C. B. Edwards, S. Hancock, M. H. Key, R. Mahadeo, M. R. G. Miller, P. A. Norreys, C. E. Ollman, D. A. Pepler, D. A. Rodkiss, I. Ross, M. A. Smith, P. F. Taday, W. T. Toner, K. Wigmore, T. B. Winstone, R. W. W. Wyatt, A. Luan, F. Beg, A. Bell, A. E. Dangor, M. H. Hutchinson, P. Lee, I. P. Mercer, R. A. Smith, F. Zhou, and A. P. Fews, in *Short-Pulse High-Intensity Lasers and Applications II,* edited by Jeffrey A. Paisner, SPIE Proc. Vol. 1860 (SPIE, Bellingham, WA, 1993), p. 10.

[23] A. K. Dave and G. J. Pert, J. Phys. B **17**, 4953 (1984).

[24] D. C. Eder, Phys. Fluids B **1**, 2462 (1989).

[25] G. J. Pert, J. Phys. B **9**, 3301 (1976); **12**, 2067 (1979); Plasma Phys. Controlled Fusion **27**, 1427 (1985).

[26] M. H. Key, Rutherford Appleton Laboratory Report No. RAL-89-045, 1989 (unpublished); Rutherford Appleton Laboratory Report No. RAL-87-041, 1987 (unpublished).

[27] J. P. Christiansen, D. E. T. F. Ashby, and K. V. Roberts, Comput. Phys. Commun. **7**, 271 (1974).

[28] A. Djaoui and S. J. Rose, J. Phys. B **25**, 2745 (1992).

[29] G. J. Rickard, A. R. Bell, and E. M. Epperlein, Phys. Rev. Lett. **62**, 2687 (1989).

[30] J. Zhang and M. H. Key, J. Appl. Phys. **74**, 7606 (1993).

[31] D. W. Forslund, J. M. Kindel, and K. Lee, Phys. Rev. Lett. **39**, 284 (1977).

[32] G. J. Tallents, L. Dwivedi, Y. Kato, M. H. Key, R. Kodama, J. Krishnan, C. L. S. Lewis, K. Murai, P. A. Norreys, G. J. Pert, S. A. Ramsden, H. Shiraga, C. Smith, J. Uhomoibhi, G. Yuan, and J. Zhang, in *X-Ray Lasers 1992,* edited by E. E. Fill (IOP, Bristol, 1992), p. 101.

[33] J. Zhang, M. H. Key, P. Norreys, and G. Tallents, Opt. Commun. **95**, 53 (1993); J. Zhang, L. Dwivedi, Y. Kato, M. H. Key, R. Kodama, J. Krishnan, C. L. S. Lewis, K. Murai, P. A. Norreys, G. J. Pert, S. A. Ramsden, H. Shiraga, C. Smith, G. J. Tallents, J. Uhomoibhi, and G. Yuan, in *X-Ray Lasers 1992* (Ref. [32]), p. 339.

[34] G. J. Linford, E. R. Peressini, W. R. Sooy, and M. L. Spaeth, Appl. Opt. **13**, 379 (1974).

[35] N. H. Burnett and G. D. Enright, IEEE J. Quantum Electron. **26**, 1797 (1990).

[36] J. P. Matte and J. Virmont, Phys. Rev. Lett. **49**, 1936 (1982).

[37] M. H. Key, S. J. Rose, N. Tragin, and J. Zhang, Opt. Commun. **98**, 95 (1993).